International Forum on Aeroelasticity and Structural Dynamics
IFASD 2017
25-28 June 2017 Como, Italy

INVESTIGATION OF FREQUENCY LOCK-IN PHENOMENA ON A SUPERCRITICAL AEROFOIL IN THE PRESENCE OF TRANSONIC SHOCK OSCILLATIONS

Nicholas F. Giannelis[1] **and Gareth A. Vio**[1]

[1]School of Aerospace, Mechanical and Mechatronic Engineering
The University of Sydney, NSW 2006, Sydney, Australia
nicholas.giannelis@sydney.edu.au
gareth.vio@sydney.edu.au

Keywords: transonic shock buffet, unsteady aerodynamics, frequency lock-in

Abstract: Within a narrow band of the transonic flight regime, shock-wave/boundary layer interactions yield large amplitude, self-sustained shock oscillations. When this transonic buffet instability interacts with a forced or freely oscillating structure, frequency lock-in between the aerodynamic and structural modes can occur, resulting in large amplitude limit cycle oscillations of the structure. In this study, the lock-in phenomenon is investigated by means of Reynolds-Averaged Navier-Stokes simulations. Harmonically driven pitching simulations are performed for a range of driving frequencies and amplitudes for the supercritical OAT15A aerofoil section. The results show that for a band of driving frequencies near the buffet, frequency synchronisation develops for sufficient driving amplitudes. The flow topology within the lock-in regions differs for driving frequencies above and below the buffet. This is attributed to a phase reversal of the aerodynamic coefficients as the excitation frequency passes through the fundamental flow frequency. Analysis of the gain and phase relationships of the aerodynamic coefficients supports the findings of prior studies, where the lock-in phenomenon is related to bounded single degree-of-freedom flutter.

1 INTRODUCTION

For a limited set of flight conditions in the transonic flight regime, the interactions between shock-waves and thin, separated shear layers give rise to large amplitude, autonomous shock oscillations. This transonic buffet instability is a limiting factor in aircraft performance. The reduced frequency of shock oscillation is typically on the order of the low-frequency structural modes, resulting in an aircraft that is susceptible to limit cycle oscillations (LCO), and as a consequence, diminished handling quality and fatigue life [1, 2].

Hilton & Fowler [3] first observed transonic shock-induced oscillations over six decades ago, yet the physics governing this complex phenomenon remains elusive. In the early work by Pearcey [4], shock buffet onset was linked to the bursting of a shock-induced separation bubble, a condition that has since been determined insufficient for the emergence of shock-induced oscillations [5,6]. Lee [7] proposed an underlying mechanism based on acoustic wave-propagation feedback, which has resulted in excellent predictions of the buffet frequency for a subset of aerofoils [8, 9] and poorer estimates for others [10, 11]. A promising theory governing the onset of shock buffet has been posited by Crouch et. al. [6, 12], where linear stability analysis of the flowfield has related autonomous shock oscillations to the appearance of a globally unstable

aerodynamic mode. Significant support of this modal instability interpretation has been offered by subsequent experimental [10, 13] and computational [5, 14] investigations. For a complete review of recent developments in the understanding of transonic shock buffet, the reader is directed to Giannelis et. al. [15].

The complex shock-wave/boundary layer interactions and the intermittently separated flowfield inherent to the transonic buffet phenomenon pose significant challenges to numerical simulation. In particular, the fundamental role of the separated flow region within these interactions implies the necessity of computationally taxing scale-resolving simulations to model the instability. Nonetheless, a plethora of computational investigations have successfully captured the inherent flow features of shock-induced oscillations through Unsteady Reynolds-Averaged Navier-Stokes (URANS) methods, albeit with an appreciable sensitivity to various simulation parameters [14, 16–21]. In particular, the selection of a suitable turbulence closure [19, 22–24], sufficient grid refinement in the shock region [20, 25, 26] and the use of Dual Time Stepping (DTS) with an acoustic temporal resolution [25, 27] have been shown to be critical in URANS modelling of transonic shock buffet. Ultimately, the efficacy of URANS simulations in the prediction of transonic buffet is attributed to the low frequencies characteristic of shock motion, which exhibit significantly longer timescales than those of the shear layer eddies [14]. Such a success for a computationally efficient means of simulating intricate aerodynamic phenomena holds promise for the numerical investigation of the complex interaction mechanisms between a buffeting flowfield and a deforming structure.

A number of experimental studies have considered the influence of forced harmonic motions on an aerofoil at transonic conditions [28–31]. Additionally, for harmonic excitation in the presence of shock-induced separation, a number of authors have reported aerodynamic resonance for driving frequencies near to the fundamental frequency of shock oscillation [32–34]. The nature of this resonance has been formalised by Raveh [35–37] as a frequency *lock-in* phenomenon, whereby for sufficient amplitudes of motion at excitation frequencies in the vicinity of the buffet frequency, the buffet flow response synchronises with the aerofoil motion. Raveh & Dowell [38] extended the work on shock buffet lock-in to spring-suspended aeroelastic systems, finding synchronisation of the aerodynamic and structural eigenfrequencies in pitch, heave and coupled simulations. As a significant implication of these findings, the authors propose shock buffet lock-in as a possible mechanism governing transonic LCO instabilities. Through linear stability analysis, Gao et. al. [39] have proposed the emergence of lock-in is not a consequence of a pure resonance phenomenon. Rather, frequency synchronisation arises due to a form of single degree-of-freedom flutter, stemming from the coupling between a structural system and an unstable fluid mode. Recent literature in the field has continued the exploration of aeroelastic systems in the presence of shock buffet, concentrating on classifying the influence of various structural parameters, particularly the ratio of structural and shock oscillation eigenfrequencies, on the lock-in phenomenon [40–44].

In the work of Giannelis & Vio [40], lock-in was observed for an elastically suspended OAT15A supercritical aerofoil in pitch and heave at structural eigenfrequencies above and below the rigid aerofoil fundamental shock frequency, respectively. The purpose of this study is to investigate the origins of this frequency synchronisation phenomenon, and to ascertain whether the simplified gain-phase model for lock-in of a harmonically excited NACA 0012 proposed by Raveh [35] is valid for supercritical wing sections. The article proceeds in Section 2 with a description of the test case and the numerical solution employed in the static aerofoil simulations. Section 3 then presents the main results for the static aerofoil, including validation of the

turbulence models against experimental data and the nature of the buffeting flowfield at the experimental condition. In Section 4, the methodology used in the dynamic simulations is briefly presented, followed by time and frequency domain analysis of the aerodynamic coefficients, investigation of the flow topology and the validity of the gain-phase lock-in relationship for a supercritical aerofoil. Section 5 then concludes the paper with a summary of the major findings.

2 NUMERICAL METHOD

2.1 Test case

This study investigates the flowfield around the OAT15A supercritical aerofoil at transonic buffet conditions. Experiments on this section have been performed in the S3Ch Continuous Research Wind Tunnel at the ONERA Chalais-Meudon Center and are detailed by Jacquin et. al. [10, 45]. A wind tunnel model of 12.3% relative thickness, 230 mm chord, 780 mm span and a 1.15 mm thick trailing edge was constructed for the experiment. The model ensured a fixed boundary layer transition at 7% chord through the installation of a carborundum strip on the upper and lower surfaces.

The experiments conducted at ONERA sought to develop an extensive experimental database for the validation of numerical buffet simulations. The model was fitted with 68 static pressure orifices and 36 unsteady Kulite pressure transducers through the central span to mitigate three-dimensional effects from sidewall boundary layers. Adaptable upper and lower wind tunnel walls further alleviated wall interference, allowing for a test section Mach number uncertainty of 10^{-4}. The investigation applied a sublimating product to the model surface, permitting oil flow visualizations for characterisation of turbulent regions and shock motion. The authors employed Schlieren cinematography and Laser Doppler Velocimetry (LDV) to observe qualitative flow features during the buffet cycle. Further, steady and unsteady pressure measurements yield mean and RMS pressure data, along with spectral content for the pressure fluctuations.

The test programme undertaken by Jacquin et. al. [10] consisted of an angle of attack sweep at $M = 0.73$ to obtain data for buffet onset, as well as Mach number sweeps at $\alpha_m = 3^\circ$ and $\alpha_m = 3.5^\circ$. In this study, the data at $M = 0.73$ and $\alpha_m = 3.5^\circ$ are employed to validate the numerical method. This case is used as a baseline from which dynamic simulations of a harmonically excited OAT15A aerofoil are developed.

2.2 Flow solver

Simulations are performed using the commercial, cell-centred finite volume code ANSYS Fluent. The two-dimensional density-based implicit solver is used to formulate the coupled set of continuity, momentum and energy equations. The inviscid fluxes are resolved by an upwind Roe flux difference splitting scheme with the blended central-difference/second-order upwind MUSCL scheme for extrapolation of the convective quantities. All diffusive fluxes are treated with a second-order accurate central-difference scheme. Gradients for the convection and diffusion terms are constructed through a cell based Least Squares method and solved by Gram-Schmidt decomposition of the cells coefficient matrix.

Three turbulence models are considered for closure of the Navier-Stokes equations; the Spalart-Allmaras model (SA) [46], Menter's $k - \omega$ SST [47] and the Stress-Omega Reynolds Stress Model (SORSM), a stress-transport model derived from the omega equations and the Launder-Reece-Rodi (LRR) model [48]. The SA and SST models have been used extensively in URANS

buffeting simulations, successfully capturing the bulk flow buffeting features. Reynolds Stress Models (RSM) have been less widely applied in the available shock buffet literature, however Illi et. al. [26] observed excellent correlations to the OAT15A experimental data set using a ϵ^h RSM model. The SORSM is derived by taking the second-moments of the exact momentum equations, yielding an additional four transport equations for the Reynolds stresses, together with an equation for the dissipation rate. All turbulent transport equations are solved segregated from the coupled set of continuity, momentum and energy equations, with second-order accurate upwind discretisation of the turbulent quantities.

2.3 Spatial & temporal discretisation

Calculations in this study are performed on a two-dimensional CH-type structured grid (Figure 1(b)) with far-field boundaries located 80 chord lengths from the profile, as shown in Figure 1(a). The domain is divided into two zones; a laminar region upstream and along 7% of the aerofoil chord forward section and a turbulent region in the remainder of the domain to represent the experimentally imposed boundary layer transition.

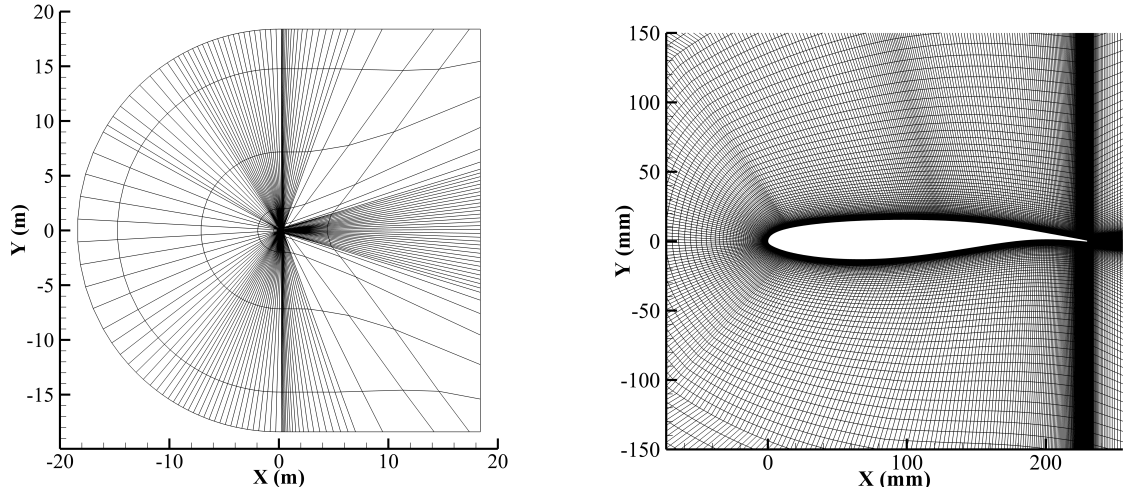

(a) Far-field grid topology

(b) Near wall grid topology - Grid C

Figure 1: Computational grid.

Three grids have been generated to assess mesh independence, with the grid parameters provided in Table 1. Refinement levels are primarily dictated by shock resolution across the aerofoil surface, with minor refinement adopted in the wall normal direction. A wall $y^+ \approx 1$ is achieved at each level of refinement. Grid convergence is assessed based upon steady flow pressure distributions at $M = 0.73$ and $\alpha_m = 2.5°$ using the SA turbulence model. Mesh independent solutions are achieved with Grid B and thus, this grid is employed for all subsequent simulations. Grid B is comprised of 285 nodes along each surface of the aerofoil profile, 96 nodes in the wake and 92 nodes in the wall normal direction.

Grid	Size ($i \times j$)	Shock Resolution (c)
A	288×86	0.005
B	381×92	0.0035
C	472×98	0.0025

Table 1: Computational grid properties.

For time-accurate solutions, an implicit second-order accurate backward Euler DTS scheme is used. A maximum Courant-Friedrichs-Lewy (CFL) number of five is imposed for the pseudo-time stepping at each physical time step. During the developed buffet cycle, a minimum of 10 Newton sub-iterations are required to reduce the L1 norm of the residuals to 10^{-5}. In order to resolve the propagating pressure waves inherent to the shock oscillation phenomenon, near acoustic temporal resolution is required. As such, a fixed nondimensional time step of $\Delta\bar{t} = 0.01$ is used in all time-accurate solutions.

3 STATIC AEROFOIL COMPUTATIONS

3.1 Turbulence modelling

The choice of the turbulence model used to explore the buffeting flow of the OAT15A aerofoil is made based on correlations to the experimental mean and RMS pressure data, in addition to the predicted buffet frequency and lift differential. In Figure 2 the mean and RMS pressure coefficients for each of the turbulence models are given. Each of the closures results in shock unsteadiness at the experimental conditions, albeit with varying degrees of accuracy. The SA model severely under-predicts the degree of pressure fluctuation due to shock oscillation, as evident in the abrupt pressure recovery in Figure 2(a) and small amplitude RMS pressure in Figure 2(b). Conversely, the RSM model overestimates the magnitude of pressure fluctuations due to shock motion, along with the range of shock travel, which covers approximately 30% of the chord. The mean pressure distribution and trailing edge pressure fluctuations are, however, in fair agreement with experiment. Nonetheless, of the three closures considered the SST model exhibits the best correlation to the experiment. The mean pressure distribution is in excellent agreement, and whilst the amplitude of pressure fluctuations due to shock motion and trailing edge separation are slightly underestimated, the range of shock travel and mean shock location is well captured.

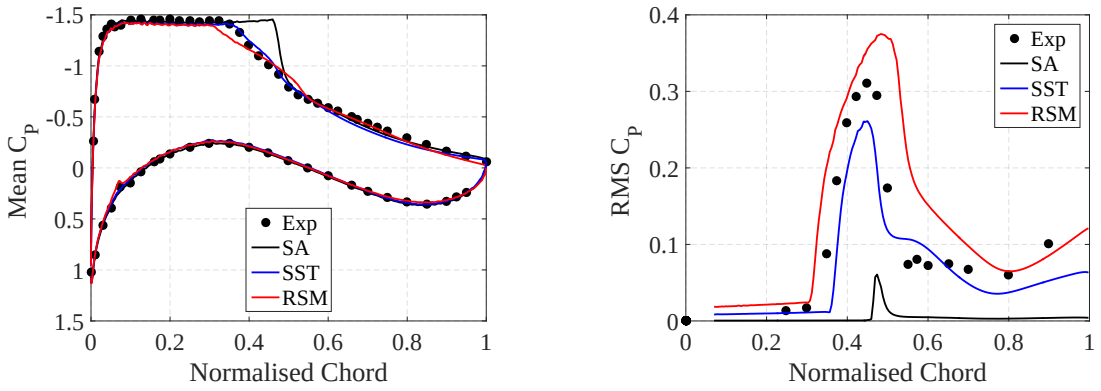

(a) Mean pressure coefficient

(b) RMS pressure coefficient

Figure 2: Pressure correlations for various turbulence models.

In addition to the pressure data, the various turbulent closures are also assessed for accuracy of the predicted buffet frequency and lift differential. The resultant buffet characteristics are given in Table 2. Each of the models yields a higher buffet frequency relative to the experiment; however, with a maximum deviation of approximately 10%, the buffet frequency is generally predicted well. The best agreement to the experimental frequency is achieved with the SST closure, exhibiting a deviation of 5%. The SST model also produces fair agreement in the peak-to-peak lift differential during the buffet cycle. This model is deemed to best represent

the experimental buffet conditions, capturing both the shock oscillation and alternating trailing edge separation inherent to transonic buffet. As such, the remainder of this study proceeds with the SST closure.

	f_{sb} (Hz)	ΔC_L
SA	74.18	0.01
SST	72.55	0.15
SORSM	74.07	0.33
Exp	69	0.11

Table 2: Computed buffet characteristics.

3.2 Buffet response at experimental conditions

The lift coefficient time and frequency responses at $M = 0.73$ and $\alpha_m = 3.5°$ are provided in Figure 3. The time history in Figure 3(a) shows the lift oscillations of the fully developed buffeting flow. Lift is seen to oscillate in a Period-1 LCO of constant amplitude, with no pronounced nonlinear effects. This is further evident in Figure 3(b), where the frequency content is concentrated at the buffet frequency for the fully developed buffeting flow. Minor peaks are also observed at the second and third harmonic of the buffet frequency; however, they exhibit insufficient power to influence the time history. The periodic nature of the buffet observed at these conditions is characteristic of Type A shock buffet as described by Tijdeman & Seebass [49].

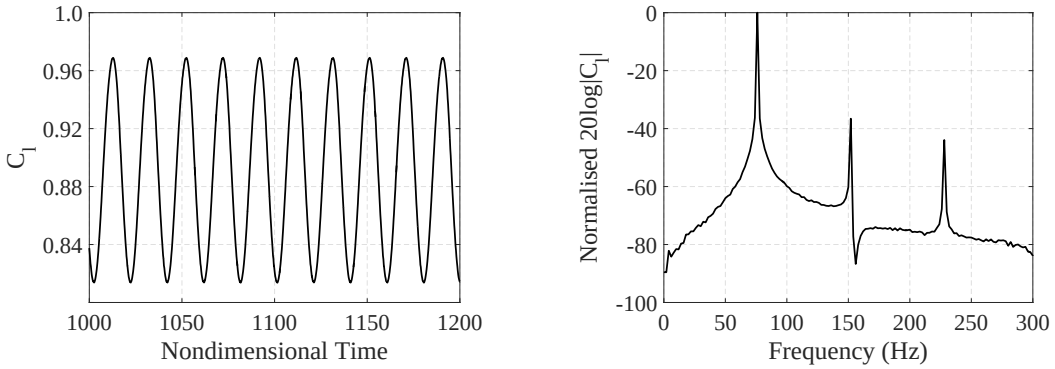

(a) C_L Time history (b) C_L Frequency response

Figure 3: Lift coefficient time & frequency responses at $M = 0.73$ & $\alpha_m = 3.5°$.

4 DYNAMIC AEROFOIL COMPUTATIONS

To investigate the lock-in behaviour of the OAT15A aerofoil, the aerofoil is excited harmonically in pitch for a range of amplitudes in the frequency band $0.5f_{sb} < f < 2f_{sb}$, where f represents the pitch driving frequency and f_{sb} is the rigid aerofoil buffet frequency. The simulations are performed at the nominal buffet condition, namely $M = 0.73$, $Re = 3 \times 10^6$ and a mean angle of attack $\alpha_m = 3.5°$. In Figure 4, typical time history and frequency responses of the lift coefficient for different driving amplitudes are shown. At low amplitudes, the aerodynamic response is aperiodic. Observing the frequency response in Figure 4(b), substantial frequency content is evident at both the buffet and driving frequencies (in addition to several sub- and super-harmonics). As the excitation amplitude grows, frequency content shifts away from the buffet frequency as the aerodynamic response begins to synchronise with the aerofoil motion. From both the time histories in Figure 4(a) and frequency responses in Figure 4(b), the

lift coefficient shows an increasingly harmonic character as the driving amplitude increases. At an excitation amplitude of $\alpha = 2°$, lock-in of the aerodynamic response to the driving frequency is clearly evident, with frequency content only present at the excitation frequency.

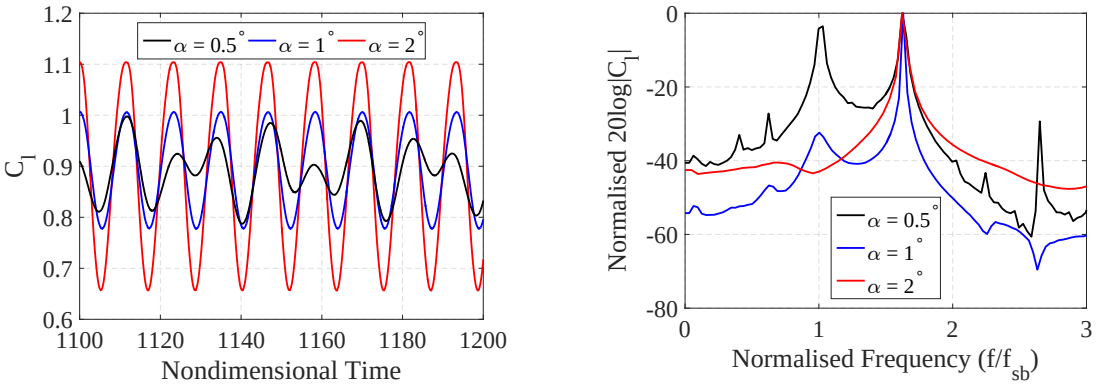

(a) Time history (b) Frequency response

Figure 4: Time and frequency responses: $f = 1.65 f_{sb}$.

In the analysis of frequency lock-in during forced oscillation of the NACA 0012 aerofoil, Raveh & Dowell [36] found that although synchronisation occurs at driving frequencies both above and below the buffet, the topology of the flowfield varies significantly between the two cases. Similar findings are presented here for the OAT15A aerofoil. In Figure 5, Mach number contours and flow streamtraces are shown at various time instances over a pitching cycle with frequency $f = 1.15 f_{sb}$ and amplitude $\alpha = 2°$. At these conditions, the aerodynamic response has synchronised with the aerofoil motion and frequency responses indicate frequency content concentrated at the pitch fundamental frequency.

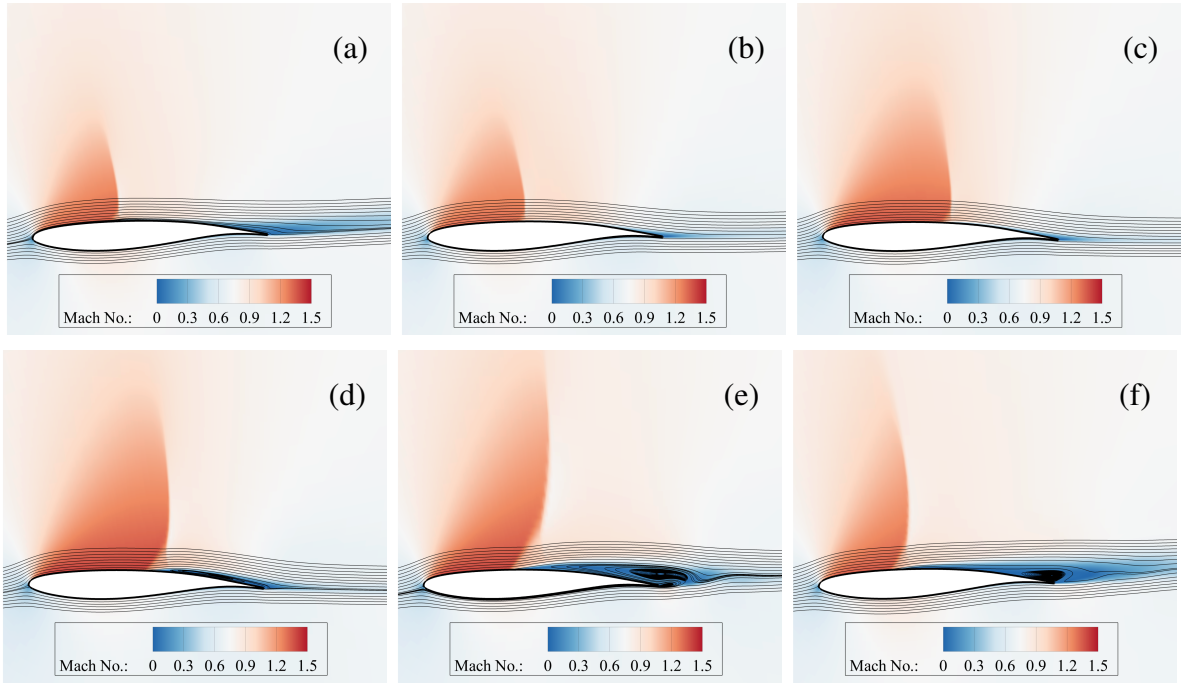

Figure 5: Mach contours and streamtraces for pitching aerofoil motion of $f = 1.15 f_{sb}$ and $\alpha = 2°$. (a) Beginning of pitch cycle; (b) 17% of pitch cycle; (c) 33% of pitch cycle; (d) 50% of pitch cycle; (e) 66% of pitch cycle; (f) 83% of pitch cycle.

The shock cycle shown in Figure 5 is indicative of Tijdeman [49] Type A shock motion. The shock traverses the suction surface of the aerofoil in a sinusoidal motion, diminishing in strength during upstream excursions. The increase in shock strength during downstream convection produces a shock-induced separation bubble (Figure 5(d)), with the extent of the separated recirculation zone growing as the shock moves upstream. The qualitative flow features are analogous to the buffet cycle of the rigid aerofoil. This differs somewhat from the findings of Raveh & Dowell [36], where the pronounced vortex shedding of the rigid aerofoil at nominal buffet conditions was quenched by imposed aerofoil motions at frequencies exceeding the buffet. It is important to note, however, that the nominal buffet condition considered here is at an incidence marginally above onset, where the rigid aerofoil does not exhibit vortex shedding. This indicates a likely dependence between the topological flow effects of shock buffet lock-in and the mean flow conditions. Further analysis with a nominal condition deep within the buffet region is required to classify this dependence.

At excitation frequencies below the buffet, the shock cycle is consistent with findings for the NACA 0012 [36]. The Mach contours and corresponding streamtraces at various instances over the oscillation cycle with frequency $f = 0.8f_{sb}$ and amplitude $\alpha = 2^\circ$ are shown in Figure 6. The shock motion at these conditions is no longer harmonic, with the emergence of a secondary shock evident during the downstream excursion in Figure 6(b). This is accompanied by an increase in shock travel and larger variations in shock strength, in addition to a more pronounced thickening of the separated recirculation zone relative to Figure 5. Although lock-in is present for both $f = 0.8f_{sb}$ and $f = 1.15f_{sb}$, there is an apparent shift in the mechanism governing shock dynamics between these two cases. This mechanism appears to be consistent between the supercritical geometry studied in the present work and the symmetrical NACA 0012 studied by Raveh & Dowell [36].

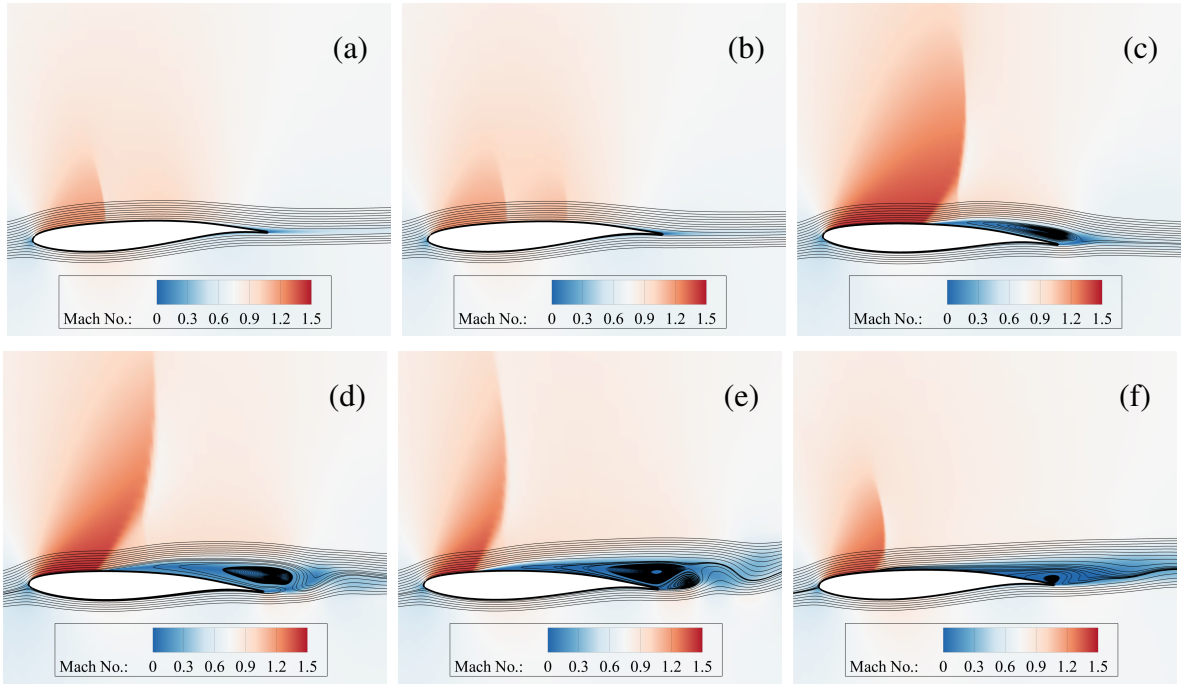

Figure 6: Mach contours and streamtraces for pitching aerofoil motion of $f = 0.8f_{sb}$. (a) Beginning of pitch cycle; (b) 12% of pitch cycle; (c) 46% of pitch cycle; (d) 58% of pitch cycle; (e) 69% of pitch cycle; (f) 81% of pitch cycle.

In Figure 7, a map of the lock-in region across different excitation amplitudes and frequencies is shown. At conditions marked with response at motion frequency, the aerodynamic coefficients exhibit frequency content primarily at the driving frequency, although both sub- and superharmonics of this excitation frequency are also present. The general trends are again consistent with prior findings for the NACA 0012 [35,36], where the extent of the lock-in frequency band grows as the excitation amplitude increases. As noted by several authors [34–36], such behaviour is similar to the synchronisation of vortex shedding frequency for an oscillating cylinder in low Reynolds number flows [50, 51]. For these flows, the onset of lock-in is attributed to classical resonance, where peak amplitude oscillations occur for excitations near the fundamental flow frequency. Additionally, the lock-in region is predominantly symmetric about this natural frequency. As shown in Figure 7, this symmetric character does not extend to oscillating aerofoils in the presence of transonic shock buffet. Frequency synchronisation appears to favour higher frequency excitations, with an apparent minimum frequency ratio of $f = 0.62 f_{sb}$ necessary for the onset of lock-in for all amplitudes considered.

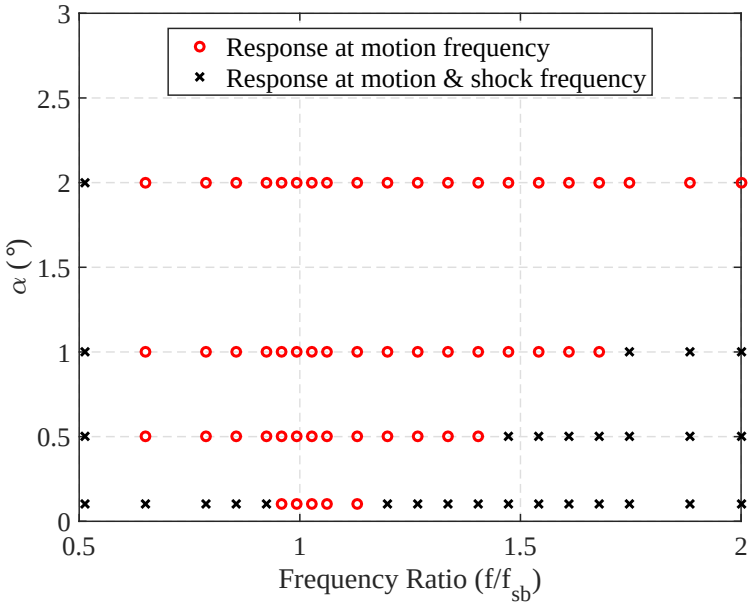

Figure 7: Map of lock-in region.

Raveh [35] proposed a simplified gain-phase relationship to represent the lock-in behaviour of an oscillating NACA 0012 aerofoil at developed buffet conditions. The applicability of this model to the supercritical OAT15A aerofoil is examined in the present work. The gain and phase relationships of the lift and pitching-moment coefficients are extracted from the aerodynamic time histories, assuming that the responses contain a single harmonic at the excitation frequency. This is a fair assumption within the lock-in region, and although higher harmonics of the driving frequency are evident in the frequency responses, their frequency content is typically below an order of magnitude of the fundamental. Under this assumption, the gain and phase of the lift and pitching-moment slope at various frequencies within the lock-in region is computed from the Lissajous curves of the aerodynamic coefficients.

In Figures 8 and 9, the resultant gain and phase relations between excitation frequency and lift and pitching-moment slope, respectively, are shown for various excitation amplitudes. The trends are consistent with the findings of Raveh [35], and indicative that the frequency synchronisation observed on the NACA 0012 is not limited to symmetric sections, extending at the least to supercritical aerofoils. The gain plots show that an increase in excitation amplitude is

accompanied by a reduction in amplification factor, in addition to a narrowing of the amplification peak. In this sense, the aerodynamic response approaches the expected resonant behaviour of a single degree-of-freedom oscillator as the perturbation amplitudes are reduced, reflecting similar characteristics to those identified by Nitzsche [5] at pre-buffet flow conditions.

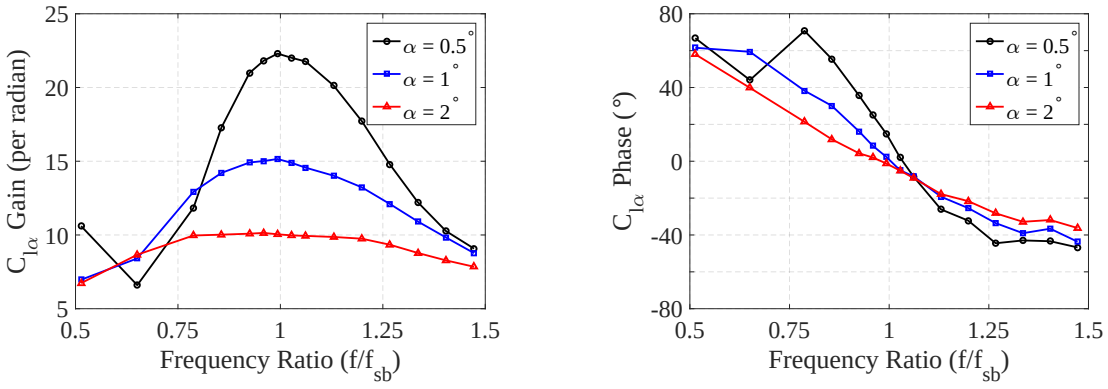

(a) Gain (b) Phase

Figure 8: Lift-curve slopes against frequency ratio.

The phase plots of the aerodynamic coefficients provide some insight into the mechanism of shock buffet lock-in for elastically suspended aerofoils. Giannelis & Vio [40] identified that for an aeroelastic OAT15A aerofoil free to rotate in pitch, frequency synchronisation (and correspondingly, large amplitude LCOs) occurred when the pitch natural frequency exceeded the buffet. For the same aerofoil free to oscillate in heave, lock-in ensued only for heave eigenfrequencies below the buffet. In reference to Figures 8(b) and 9(b), this corresponds to the frequency band in which the driving aerodynamic coefficient (pitching-moment for pitch and lift for heave) leads the structural motion. The large amplitude LCOs observed therein are thus likely a form of single degree-of-freedom flutter, where the interaction between the structural mode and an unstable fluid mode yields bounded oscillations. The linear stability analysis performed by Gao et. al. [39] confirmed this to be the mechanism governing lock-in of the NACA 0012. Additionally, the phase reversal of both pitching-moment and lift coefficient as the excitation frequency passes through the fundamental buffet frequency offers an explanation for the shift in shock dynamics with driving frequencies above and below the buffet.

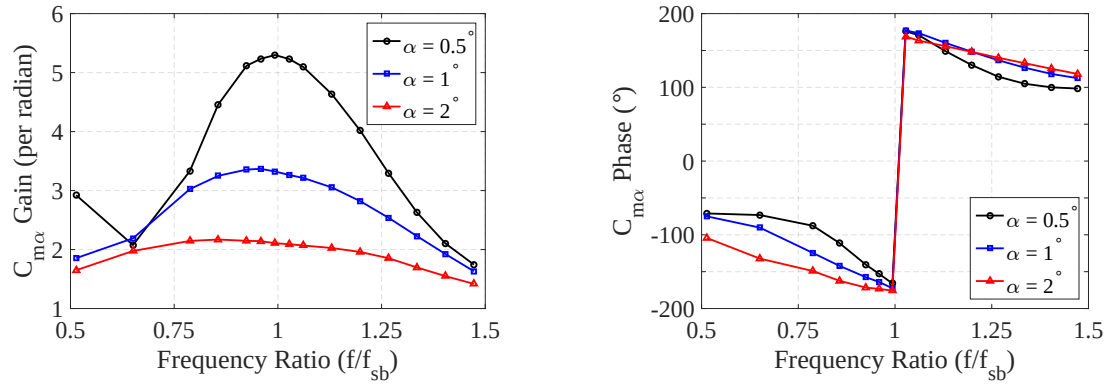

(a) Gain (b) Phase

Figure 9: Moment-curve slopes against frequency ratio.

5 CONCLUSIONS

In this paper, the transonic buffeting flow over the OAT15A supercritical aerofoil has been analysed through URANS simulation. Grid independence is assessed relative to a steady flow pre-buffet condition and is achieved with a medium density grid. Following spatial convergence, various turbulence models are considered for the time-accurate solutions. It is found that Menter's SST model yields unsteady solutions that correlate well with the experimental results. The buffeting flowfield at the experimental condition has been analysed, and is shown to be characteristic of Type A shock motion, with periodic shock excursions along the upper surface.

Dynamic simulations at the experimental flow conditions have also been performed, with harmonic excitations of the OAT15A aerofoil across a range of driving frequencies and amplitudes. Frequency synchronisation of the aerodynamic coefficients with the structural motion has been observed for sufficiently large amplitude pitching motions at frequencies near the fundamental flow frequency. The frequency band for which lock-in occurs is found to be asymmetric about the rigid aerofoil buffet frequency, with synchronisation extending farther into the higher frequency range. Distinct topological flow features have also been identified, which depend on the ratio of excitation to buffet frequencies. At higher frequencies, the shock cycle resembles that of the rigid aerofoil, with sinusoidal shock motion across the suction surface. The buffet cycle at lower excitation frequencies no longer exhibits a harmonic character. A secondary shock is observed during downstream excursions, with the extent of shock motion and separated flow regions exacerbated.

The shift in character of the buffet cycle is related to the phase reversal of the aerodynamic coefficients as the driving frequency passes through the buffet. A simplified gain-phase model analogous to that proposed by Raveh [35] is fit to the simulation data and reveals qualitatively similar behaviour of the lock-in mechanism for the supercritical aerofoil studied herein. The findings support the mechanism governing transonic limit cycles of aircraft structures proposed in previous studies. For pitch natural frequencies in excess of the buffet, the pitching-moment coefficient leads the structural motion and drives the development of large-scale bounded oscillations. For systems free to oscillate in heave, the lock-in phenomenon occurs at structural frequencies below the buffet, where the lift coefficient leads the structure. To further examine this behaviour, a future study will investigate the linearised eigenspace of an elastically suspended OAT15A aerofoil, in a similar light to the stability analysis performed by Gao et. al. [39].

6 REFERENCES

[1] Taylor, N. V., Allen, C., Gaitonde, A. L., et al. (2006). Aeroelastic analysis through linear and non-linear methods: a summary of flutter prediction in the PUMA DARP. *The Aeronautical Journal*, 110(1107), 333–343.

[2] Cooper, J. E., Miller, S., Sensburg, O., et al. (2008). Optimization of a scaled sensorcraft model with passive gust alleviation. In *Proceedings of the 12th AIAA/ISSMO Multidisciplinary Analysis and Optimization Conference*.

[3] Hilton, W. F. and Fowler, R. G. (1947). Photographs of shock wave movement. NPL R&M No. 2692, National Physical Laboratories.

[4] Pearcey, H. H. (1958). A method for the prediction of the onset of buffeting and other separation effects from wind tunnel tests on rigid models. AGARD TR 223, National Physics Laboratory.

[5] Nitzsche, J. (2009). A numerical study on aerodynamic resonance in transonic separated flow. In *Proceedings of the International Forum on Aeroelasticity and Structural Dynamics, Seattle, WA*.

[6] Crouch, J. D., Garbaruk, A., Magidov, D., et al. (2009). Origin of transonic buffet on aerofoils. *Journal of Fluid Mechanics*, 628, 357–369.

[7] Lee, B. H. K. (1990). Oscillatory shock motion caused by transonic shock boundary-layer interaction. *AIAA Journal*, 28(5), 942–944.

[8] Lee, B. H. K. (2001). Self-sustained shock oscillations on airfoils at transonic speeds. *Progress in Aerospace Sciences*, 37(2), 147–196.

[9] Xiao, Q., Tsai, H. M., and Liu, F. (2006). Numerical study of transonic buffet on a supercritical airfoil. *AIAA Journal*, 44(3), 620–628.

[10] Jacquin, L., Molton, P., Deck, S., et al. (2009). Experimental study of shock oscillation over a transonic supercritical profile. *AIAA Journal*, 47(9), 1985–1994.

[11] Garnier, E. and Deck, S. (2010). Large-eddy simulation of transonic buffet over a supercritical airfoil. In *Direct and Large-Eddy Simulation VII*, vol. 13. ERCOFTAC Series, Springer, Heidelberg, pp. 549–554.

[12] Crouch, J. D., Garbaruk, A., and Magidov, D. (2007). Predicting the onset of flow unsteadiness based on global instability. *Journal of Computational Physics*, 224(2), 924–940.

[13] Masini, L., Timme, S., Ciarella, A., et al. (2017). Influence of vane vortex generators on transonic wing buffet: Further analysis of the BUCOLIC experimental dataset. In *Proceedings of the 52nd 3AF International Conference on Applied Aerodynamics, Lyon, France*.

[14] Sartor, F., Mettot, C., and Sipp, D. (2014). Stability, receptivity, and sensitivity analyses of buffeting transonic flow over a profile. *AIAA Journal*, 53(7), 1980–1993.

[15] Giannelis, N. F., Vio, G. A., and Levinski, O. (2017). A review of recent developments in the understanding of transonic shock buffet. *Progress in Aerospace Sciences*. doi: 10.1016/j.paerosci.2017.05.004.

[16] Levy Jr, L. L. (1978). Experimental and computational steady and unsteady transonic flows about a thick airfoil. *AIAA Journal*, 16(6), 564–572.

[17] Edwards, J. W. and Thomas, J. L. (1989). Computational methods for unsteady transonic flows. *Unsteady Transonic Aerodynamics*, 120, 211–261.

[18] Maksymiuk, C. M. and Pulliam, T. H. (1987). Viscous transonic airfoil workshop results using ARC2D. In *Proceedings of the 25th AIAA Aerospace Sciences Meeting, Reno, NV*.

[19] Goncalves, E. and Houdeville, R. (2004). Turbulence model and numerical scheme assessment for buffet computations. *International Journal for Numerical Methods in Fluids*, 46(11), 1127–1152.

[20] Iovnovich, M. and Raveh, D. E. (2012). Reynolds-averaged Navier-Stokes study of the shock-buffet instability mechanism. *AIAA Journal*, 50(4), 880–890.

[21] Grossi, F., Braza, M., and Hoarau, Y. (2014). Prediction of transonic buffet by Delayed Detached-Eddy Simulation. *AIAA Journal*, 52(10), 2300–2312.

[22] Barakos, G. and Drikakis, D. (2000). Numerical simulation of transonic buffet flows using various turbulence closures. *International Journal of Heat and Fluid Flow*, 21(5), 620–626.

[23] Brunet, V. (2003). Computational study of buffet phenomenon with unsteady RANS equations. In *Proceedings of the 21st AIAA Applied Aerodynamics Conference, Orlando, FL.*

[24] Thiery, M. and Coustols, E. (2005). URANS computations of shock-induced oscillations over 2D rigid airfoils: Influence of test section geometry. *Flow, Turbulence and Combustion*, 74(4), 331–354.

[25] Rumsey, C. L., Sanetrik, M. D., Biedron, R. T., et al. (1996). Efficiency and accuracy of time-accurate turbulent Navier-Stokes computations. *Computers & Fluids*, 25(2), 217–236.

[26] Illi, S., Lutz, T., and Krämer, E. (2012). On the capability of unsteady RANS to predict transonic buffet. In *Proceedings of the Third Symposium Simulation of Wing and Nacelle Stall, Braunschweig, Germany*.

[27] Rouzaud, O., Plot, S., and Couaillier, V. (2000). Numerical simulation of buffeting over airfoil using dual time stepping method. In *Proceedings of the European Conference on Computational Fluid Dynamics ECCOMAS CFD 2000, Barcelona, Spain*.

[28] Tijdeman, H. (1977). *Investigations of the transonic flow around oscillating airfoils*. PhD Thesis, TU Delft, Delft University of Technology.

[29] Davis, S. S. (1982). NACA 64A010 Oscillatory Pitching. Compendium of Unsteady Aerodynamics Measurements AGARD-R-702, Advisory Group for Aerospace Research and Development.

[30] Landon, R. H. (1982). NACA 0012 Oscillatory and Transient Pitching. Compendium of Unsteady Aerodynamics Measurements AGARD-R-702, Advisory Group for Aerospace Research and Development.

[31] Zwaan, R. J. (1982). NLR 7301 Supercritical Airfoil Oscillatory Pitching and Oscillating Flap. Compendium of Unsteady Aerodynamics Measurements AGARD-R-702, Advisory Group for Aerospace Research and Development.

[32] Davis, S. S. and Malcolm, G. N. (1980). Transonic shock-wave/boundary-layer interactions on an oscillating airfoil. *AIAA Journal*, 18(11), 1306–1312.

[33] Despere, C., Caruanal, D., Mignosi, A., et al. (2001). Buffet active control-experimental and numerical results. In *Proceedings of RTO AVT Symposium on Active Control Technology of Enhanced Performance Operational Capabilities of Military Aircraft, Land Vehicles, and Sea Vehicles, Braunschweig, Germany*.

[34] Hartmann, A., Klaas, M., and Schröder, W. (2013). Coupled airfoil heave/pitch oscillations at buffet flow. *AIAA Journal*, 51(7), 1542–1552.

[35] Raveh, D. E. (2009). Numerical study of an oscillating airfoil in transonic buffeting flows. *AIAA Journal*, 47(3), 505–515.

[36] Raveh, D. E. and Dowell, E. H. (2011). Frequency lock-in phenomenon for oscillating airfoils in buffeting flows. *Journal of Fluids and Structures*, 27(1), 89–104.

[37] Iovnovich, M. and Raveh, D. E. (2012). Transonic unsteady aerodynamics in the vicinity of shock-buffet instability. *Journal of Fluids & Structures*, 29, 131–142.

[38] Raveh, D. E. and Dowell, E. H. (2014). Aeroelastic responses of elastically suspended airfoil systems in transonic buffeting flows. *AIAA Journal*, 52(5), 926–934.

[39] Gao, C., Zhang, W., Li, X., et al. (2017). Mechanism of frequency lock-in in transonic buffeting flow. *Journal of Fluid Mechanics*, 818, 528–561.

[40] Giannelis, N. F. and Vio, G. A. (2016). Aeroelastic interactions of a supercritical aerofoil in the presence of transonic shock buffet. In *Proceedings of the 54th AIAA Aerospace Sciences Meeting, San Diego, CA*.

[41] Carrese, R., Marzocca, P., Levinski, O., et al. (2016). Investigation of supercritical airfoil dynamic response due to transonic buffet. In *Proceedings of the 54th AIAA Aerospace Sciences Meeting, San Diego, CA*.

[42] Quan, J., Zhang, W., Gao, C., et al. (2016). Characteristic analysis of lock-in for an elastically suspended airfoil in transonic buffet flow. *Chinese Journal of Aeronautics*, 29(1), 129–143.

[43] Giannelis, N. F., Geoghegan, J. A., and Vio, G. A. (2016). Gust response of a supercritical aerofoil in the vicinity of transonic shock buffet. In *Proceedings of the 20th Australasian Fluid Mechanics Conference, Perth, Western Australia*.

[44] Giannelis, N. F., Vio, G. A., and Dimitriadis, G. (2016). Dynamic interactions of a supercritical aerofoil in the presence of transonic shock buffet. In *Proceedings of the 27th International Conference on Noise and Vibration Engineering, Leuven, Belgium*.

[45] Jacquin, L., Molton, P., Deck, S., et al. (2005). An experimental study of shock oscillation over a transonic supercritical profile. In *Proceedings of the 35th AIAA Fluid Dynamics Conference and Exhibit, Toronto, Ont.*

[46] Spalart, P. R. and Allmaras, S. R. (1994). A one-equation turbulence model for aerodynamic flows. *La Recherche Aerospatiale*, 1(5).

[47] Menter, F. R. (1994). Two-equation eddy-viscosity turbulence models for engineering applications. *AIAA Journal*, 32(8), 1598–1605.

[48] Launder, B. E., Reece Jr, G., and Rodi, W. (1975). Progress in the development of a Reynolds-stress turbulence closure. *Journal of Fluid Mechanics*, 68(03), 537–566.

[49] Tijdeman, H. and Seebass, R. (1980). Transonic flow past oscillating airfoils. *Annual Review of Fluid Mechanics*, 12(1), 181–222.

[50] Singh, S. P. and Mittal, S. (2005). Vortex-induced oscillations at low Reynolds numbers: hysteresis and vortex-shedding modes. *Journal of Fluids and Structures*, 20(8), 1085–1104.

[51] Dowell, E. H., Hall, K. C., Thomas, J. P., et al. (2008). A new solution method for unsteady flows around oscillating bluff bodies. In *IUTAM Symposium on Fluid-Structure Interaction in Ocean Engineering*. Springer, pp. 37–44.

COPYRIGHT STATEMENT

The authors confirm that they, and/or their company or organization, hold copyright on all of the original material included in this paper. The authors also confirm that they have obtained permission, from the copyright holder of any third party material included in this paper, to publish it as part of their paper. The authors confirm that they give permission, or have obtained permission from the copyright holder of this paper, for the publication and distribution of this paper as part of the IFASD-2017 proceedings or as individual off-prints from the proceedings.